Clays and Clay Minerals, Vol. 54, No. 4, 500–514, 2006.

INFLUENCE OF MECHANICAL COMPACTION AND CLAY MINERAL DIAGENESIS ON THE MICROFABRIC AND PORE-SCALE PROPERTIES OF DEEP-WATER GULF OF MEXICO MUDSTONES

ANDREW C. APLIN[1], INGO F. MATENAAR[1,†], DOUGLAS K. MCCARTY[2] AND BEN A. VAN DER PLUIJM[3]

[1] NRG, School of Civil Engineering and Geosciences and Institute for Research on Environment and Sustainability, Devonshire Building, Newcastle University, Newcastle upon Tyne NE1 7RU, UK
[2] Chevron ETC, 3901 Briarpark, Houston, TX 77042, USA
[3] Department of Geological Sciences, University of Michigan, C.C. Little Building, 425 E. University Ave., Ann Arbor, MI 48109-1063, USA

Abstract—We report on how the effects of mechanical compaction and clay mineral diagenesis have affected the alignment of phyllosilicates in a suite of Miocene-Pliocene mudstones buried to sub-seabed depths of between 1.8 and 5.8 km in the deep-water Gulf of Mexico. Mechanical compaction has reduced the porosity of the samples to 15% at 5 km, with modal pore sizes between 10 and 20 nm. High-resolution X-ray texture goniometry data show that the intense mechanical compaction has not resulted in a strongly aligned phyllosilicate fabric. The muds were apparently deposited with a weak or isotropic phyllosilicate fabric which was not substantially realigned by mechanical compaction. Unusually, X-ray diffraction of <0.2 μm separates shows that: (1) there is no illitization trend between 90 and 120ºC; and (2) discrete smectite persists to ~120ºC, coexisting with R1 I-S or R0 I-S with 30–40% expandable layers. Between 120 and 130ºC, discrete smectite disappears and the expandability of I-S decreases to ~25–30%. We propose a two-stage diagenetic process involving (1) the alteration of volcanic glass to smectite and (2) the illitization of smectite and I-S; the alteration of glass results in smectite without a preferred orientation and retards the illitization reaction. We suggest that the lack of a strongly aligned phyllosilicate fabric reflects the apparently limited extent of illitization, and thus recrystallization, to which these mudstones have been subjected.

Key Words—Compaction, Gulf of Mexico, High-resolution X-ray Texture Goniometry, Microfabric, Mudstone, Shale, Smectite.

INTRODUCTION

Muds and mudstones are largely formed from grains <63 μm in diameter, loosely comprising a mixture of lath-shaped clay minerals and more equidimensional grains such as quartz and feldspar. Grains >10 μm (often quartz, feldspar and mica) are thought to be deposited as single grains, with grains <10 μm (mainly but not uniquely clay minerals) deposited as flocs (Kranck *et al.*, 1996a, 1996b). This depositional model implies that marine muds are likely to be deposited with an essentially isotropic fabric, an idea supported by visual observations of recent sediments (*e.g.* Bennett *et al.*, 1991). With increasing burial and thermal stress, muds are converted to metapelites, at which stage platy clay minerals are reoriented to form a strongly aligned fabric, broadly parallel to bedding (Oertel, 1983; Ho *et al.*, 1995; Jacob *et al.*, 2000). The post depositional processes that lead to the reorientation of phyllosilicate particles include both mechanical compaction (*e.g.* Hedberg, 1936; Bowles *et al.*, 1969; Bennett *et al.*, 1981; Vasseur *et al.*, 1995) and the recrystallization of clay minerals (*e.g.* Ho *et al.*, 1999; Jacob *et al.*, 2000). Qualitative, visual observations of muds both in the field and in the laboratory suggest the importance of mechanical reorientation of particles, at least during the early stages of compaction (Bowles *et al.*, 1969; Bennett *et al.*, 1981; Vasseur *et al.*, 1995). Whilst these qualitative studies have provided very useful information, more quantitative descriptions of fabric are required to compare samples and unravel processes that realign phyllosilicates. The very few studies that have used X-ray goniometry to quantify the phyllosilicate fabric of deeply buried mudstones are thus particularly important. Early studies (Oertel and Curtis, 1972; Curtis *et al.*, 1980) concluded that whilst phyllosilicates become increasingly aligned during burial diagenesis, the ratio of platy phyllosilicates to more equidimensional quartz influences the extent to which a strong fabric is developed. Unfortunately, the sample sets analyzed within these isolated studies did not allow the authors to differentiate the roles of (1) mechanical compaction and (2) clay mineral recrystallization in the rearrangement of mudstone fabric. More recently, however, Ho *et al.* (1999) used high-resolution X-ray texture goniometry (HRXTG) to show a

* E-mail address of corresponding author:
a.c.aplin@ncl.ac.uk
† Present address: ExxonMobil Exploration Company, 222 Benmar Drive, Houston, Texas 77060, USA
DOI: 10.1346/CCMN.2006.0540411

substantial increase in the alignment of clay minerals as a result of the smectite-to-illite transition in the onshore Gulf of Mexico.

In this study we use HRXTG to quantify the alignment of phyllosilicates in a series of mudstones deposited in the deep-water (1.5–2 km) Gulf of Mexico and buried to depths of between 1.8 and 5.8 km below the seafloor. Our main aims were to investigate the extent to which phyllosilicates are rotated and realigned as a function of (1) mechanical compaction and (2) clay mineral diagenesis.

SAMPLES

In an ideal world, diagenetic studies are performed on samples which were identical at the sediment-water interface and then buried differentially to the appropriate range of temperature and pressure. Since this is unrealistic or impossible, compromise is essential and generally involves selecting material either of different ages from a single well and/or of similar age from several wells. In this study, we have chosen samples from three wells (code-named Panis, Ikon and Diva) in the deep-water Gulf of Mexico, all of which received sediment from the paleo Mississippi River. Based on paleontological data supplied by the oil companies which drilled the wells, most of the samples are Miocene in age, with Pliocene samples in the upper part of Panis. Panis is situated in the Green Canyon area of the Gulf of Mexico; Ikon and Diva are situated close to one other, ~200 km from Panis. Collectively, the three wells enabled us to select material of broadly similar age covering a sufficiently wide range of both temperature and burial depth.

Seventeen samples were taken at depths between 1816 and 5884 m below seafloor (mbsf), representing a measured, downhole temperature range of 40–130ºC (Table 1). Samples from Panis are cuttings, whereas samples from Ikon and Diva are a mixture of conventional core and rotary sidewall core. Muds comprise 80–90% of the sections in all three locations. There is insufficient information to specify detailed depositional environments for the muds, although chaotic bedding, consistent with some form of mass flow deposit, is observed in parts of the (sparse) cored sections. Several previous studies have highlighted the volumetric importance of mass flow deposits both generally within slope environments and more specifically within the deep-water part of the Gulf of Mexico (Lindsay *et al.*, 1984; Hampton *et al.*, 1996; Schwab *et al.*, 1996).

ANALYTICAL METHODS

Physical properties

Samples of cores and carefully cleaned cuttings were disaggregated by a gentle freeze-thaw procedure (Yang and Aplin, 1997). Clay fractions (percentage of particles <2 μm in diameter) were determined using a Micromeritics Sedigraph 5000ET© device, after wet-sieving the samples at 63 μm. The Sedigraph measurements were calibrated with internal standards (London Clay) which had been previously been analyzed using the pipette method (British Standards 1377, part 6, 1990).

Porosities and pore-size distributions were determined on freeze-dried samples (Delage and Lefebvre, 1984) using a Micromeritics© Autopore II 9220 mercury intrusion porosimeter. Porosities were calculated from bulk volume and measured grain density (British

Table 1. Basic physical properties.

Well	Depth (mbsf)	Sample type	Temp. (ºC)	Clay (%)	Porosity	Modal pore size (nm)
Panis	1816	ct	40	41	0.15	13
Panis	1999	ct	44	39	–	12
Panis	2907	ct	64	40	0.14	10
Panis	3090	ct	67	44	0.18	10
Ikon	4128	core	90	46	0.22	–
Ikon	4418	core	95	39	0.16	12
Ikon	5133	core	107	56	0.19	12
Ikon	5420	swc	111	44	0.17	10
Ikon	5884	swc	116	40	0.16	6 & 26
Diva	4855	swc	117	36	0.17	9
Diva	5001	core	120	49	0.17	8
Diva	5435	swc	127	39	0.14	8
Diva	5511	core	128	37	0.13	8
Diva	5516	core	128	33	0.16	10
Diva	5518	core	128	60	0.15	14
Diva	5647	core	130	22	0.09	7
Diva	5649	core	130	38	0.12	6

mbsf = meters below sea floor; ct = cutting; swc = sidewall core; Clay = mass% particles <2 μm diameter

Standard 733, 1987) and thus represent total porosity, not just the porosity into which mercury could be injected. Pore diameters were calculated from the mercury injection data assuming a mercury-air contact angle of 141° and an interfacial tension of 480 mNm^{-1}.

Mineralogy

Whole-rock X-ray diffraction (XRD) was performed on randomly oriented, ground samples. Clay fractions (<2 μm grain size) were separated in settling tubes and oriented slides were prepared for XRD using a procedure similar to the 'Millipore© Filter Transfer Method' described by Moore and Reynolds (1997). For the Panis samples, XRD was undertaken using CuKα radiation with a Hiltonbrooks DG2 X-ray generator connected to a Phillips PW1050 goniometer and a Phillips PW1752 single-crystal graphite monochromator. The step size was 0.04°2θ with a counting time of 2 s per step. The Ikon and Diva <2 μm samples were analyzed using CoKα radiation on a Siemens D5000 diffractometer equipped with a diffracted beam monochromator. In this case a step size of 0.02°2θ was used, with a counting time of 1 s per step.

Initial analysis of the <2 μm samples suggested that the main changes in the mineralogy of illite-smectite phases occurred in samples from Ikon and Diva. The <0.2 μm size fractions of the Ikon and Diva samples were therefore separated, saturated three times with 1 mol/L NaCl, dialyzed extensively and run from 2 to 45°2θ on a Siemens D5000 diffractometer, as for the <2 μm fractions. In all cases both air-dried and glycolated samples were analyzed.

XRD pattern analysis

Full-pattern computer modeling, or simulation, is probably the most effective way to reveal the structural details of complex clay mixtures involving mixed-layer phases. Structural analysis of mixed-layer clays and estimation of the relative proportions of clay types in the oriented aggregate were carried out using computer modeling or simulation of the full experimental XRD pattern (*e.g.* Drits *et al.*, 1997a, 2002; Sakharov *et al.*, 1999; McCarty *et al.*, 2004). The XRD pattern from the ethylene glycol (EG) preparation was modeled for each sample; the multi-specimen fitting technique that simulates diffraction data from both the EG and air-dried scans of the same sample was used to verify the model for at least several of the structural types found in the sample set. The result is judged to be reasonable when the best fit is obtained for both of these simulations using the same structural and probability parameters. This analysis used a proprietary computer program of Chevron Inc. called Sybilla which is similar to that of Drits and Sakharov (1976) and which has been used in many such studies. The mathematical formalisms on which the program is based can be found in Drits and Tchoubar (1990). The digital XRD data from samples analyzed with Co radiation were converted to CuKα prior to computer modeling.

In practice, the procedure involves two steps. The first uses a trial-and-error approach to determine the structural and probability parameters that provide a satisfactory agreement between experimental and calculated positions, intensities and profiles of basal reflections for each phase of the sample. At the second step, the structural and probability parameters describing each phase are fixed, and the program automatically seeks the best agreement (minimum R_{WP} factor) between the experimental and calculated patterns by varying the content of the phases in the sample. As a result, the quantities or weighted concentrations of discrete and mixed-layer phases in a sample are determined. We define layers which in the EG-solvated state swell to 16.6−16.9 Å as smectite and those which swell to 12.9−13.5 Å as vermiculite, or high-charge smectite.

For structural models of air-dried and glycolated mixed-layer minerals, the Z-coordinates of Moore and Reynolds (1997) were used while the most influential site occupancies to the overall fit, octahedral Fe and interlayer K, were found using a trial and error approach. The thicknesses of coherent scattering domains (CSDs) were log-normally distributed and the parameters of this distribution were determined using the mean thickness of CSDs and regression given by Drits *et al.* (1997b) with mean and maximum thicknesses of CSDs as variable parameters. Example patterns and fits are shown in Figure 1.

Fabric analysis by HRXTG

Mudstone samples were made into polished sections for microstructural and fabric analysis. The mudstone sections were mounted on glass slides and cut perpendicular to any visible, primary bedding structures. High-resolution backscattered electron microscopy (BSEM) was used to examine the mudstones (Jeol 6400 electron microscope operating at 20 kV and 2 nA, with a spot size of 2 mm and at a working distance of ~15 mm).

A quantitative assessment of the alignment of phyllosilicates was made on an Enraf-Nonius CAD4 automated single-crystal diffractometer using the HRXTG method described by van der Pluijm *et al.* (1994). This determines crystallographic orientations over a ~1 mm^2 area of a 200−400 μm thick rock section. Because the principal stress in these sediments is vertical, sections were cut from cores parallel to the vertical stress. For cuttings, we used a hand lens or binocular microscope to identify any depositional lamination and made a cut perpendicular to the lamination. In some cases, this proved impossible and several sections were made. Thin-sections mounted on glass slides were cut to between 200 and 400 μm and, if necessary, ground with a grinding powder of 400 grit or finer. Finally, sections were detached from the glass slides and glued to aluminum sample holders.

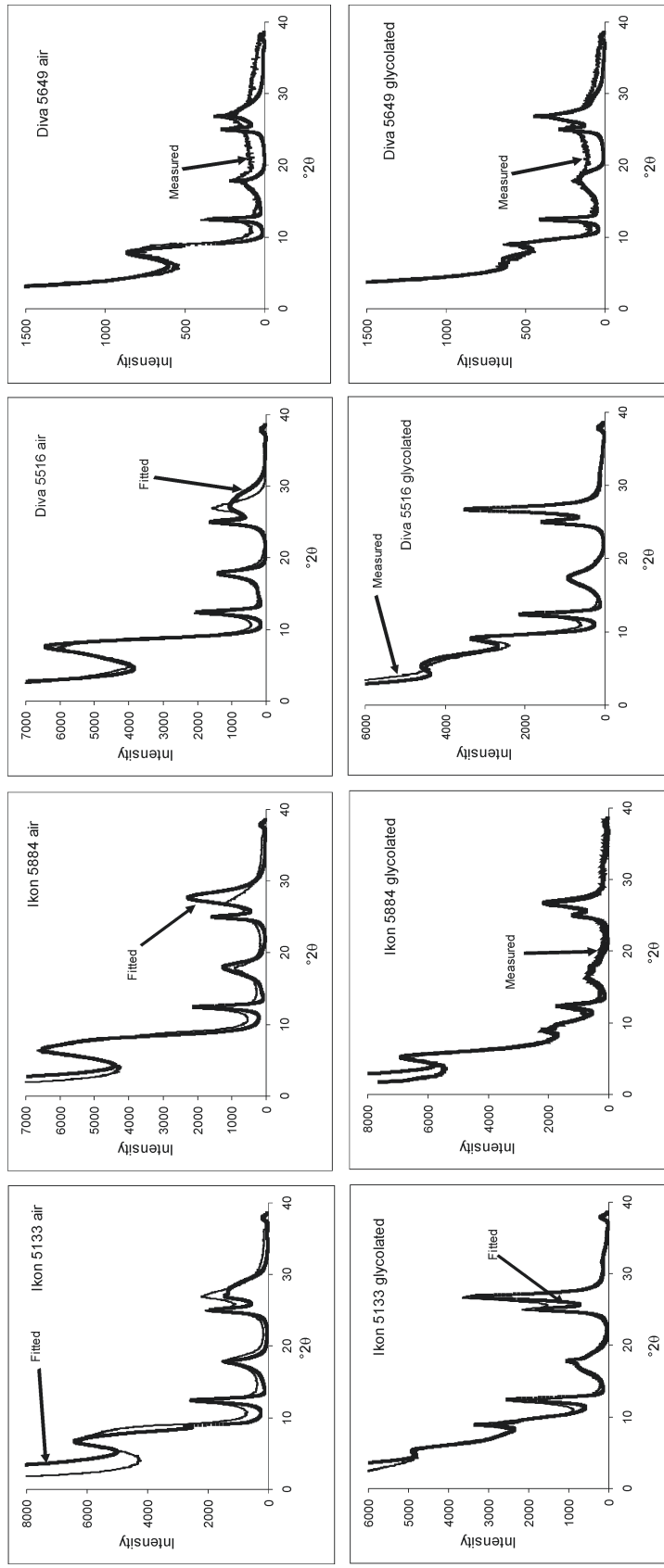

Figure 1. Experimental and simulated XRD patterns of Na-saturated, air-dried (upper) and glycolated (lower) <0.2 μm separates of four representative samples. Fits used: Ikon 5133 – 59% R1 I-S with 32% S; 17% K; 13% S; 11% I; Ikon 5884 – 64% R1 I-S with 38% S; 14% K; 16% S; 6% I; Diva 5516 - 84% R1 I-S with 33% S; 16% K; 0% S; 0% I; Diva 5649 - 85% R1 I-S with 28% S; 11% K; 0% S; 4% I. See text for details of the simulation methods.

The HRXTG analysis is a two-step process. First, the samples are scanned over the range 0.5−6.0º2θ Mo (1−13º2θ Cu). This indicates which clay mineral phases are present and determines the exact diffraction angles at which textural data should be collected. The '2θ scan' (Ho *et al.*, 1995) also allows us to consider whether the sample slab is aligned perpendicular to the predominant clay mineral fabric. An absence of peaks on the 2θ diffractograms could mean that (1) the sample is not aligned perpendicular to the main fabric direction, or (2) there are insufficient numbers of clay minerals to produce a detectable diffraction peak, or (3) the sample does not have an aligned phyllosilicate fabric. In the absence of peaks on the 2θ scan, additional sections were made in order to determine whether or not the sample has an aligned phyllosilicate fabric.

The second step of the measurement process involves the "pole-figure scan" (Ho *et al.*, 1995), in which the degree of preferred orientation of previously identified phyllosilicates is determined. The goniometer and detector are fixed at the diffraction angle corresponding to the *d* spacing of the 001 dimension of the chosen phase. Samples are then rotated around two axes, one parallel to an imaginary line connecting the goniometer and detector (designated as φ), and one normal to it (designated as ω). Diffracted X-ray intensity data are collected every 2.5º between 0 and 360º around the φ axis, and in five steps between 0 and 40º around the ω axis. In total, 1152 intensity measurements are thus made on each sample and are corrected for grain density and specimen thickness (van der Pluijm *et al.*, 1994).

The degree of alignment is obtained from the intensity distribution of diffracted X-rays. Intensity data are displayed in pole figure diagrams that show the distribution of crystallographic orientations in the form of poles to crystallographic planes. Pole figure diagrams visualize the spatial distribution of the X-ray intensities by displaying contour lines representing the pole distribution of phyllosilicate 001 orientations. More highly aligned fabrics yield pole figures that can be contoured as concentric rings; completely random or isotropic fabrics yield figures that have no poles. The degree of particle alignment is expressed as maximum pole density in multiples of a random distribution (m.r.d.), where higher values reflect higher degrees of alignment. For context, previous work on mudstones and shales (Ho *et al.* 1995, 1996, 1999, 2001; Jacob *et al.*, 2000) has generated maximum pole densities between one and seven, where values of <~2.5 indicate a very weak fabric and values >~4 indicate a strong fabric. At temperatures of >180ºC, maximum pole densities exceed 12−16 m.r.d. as cleavage is developed (Ho *et al.*, 1996; Jacob *et al.*, 2000). One single biotite crystal gave a value of 45 m.r.d. (Solum, pers. comm.).

RESULTS

Lithology and bulk mineralogy

Both clay contents and bulk mineralogy indicate the broadly similar lithological nature of many of the samples (Tables 1 and 2). Although clay contents (mass percentage of particles <2 μm in spherical diameter) vary between 22 and 60%, most samples have clay contents between 35 and 50%. There is no greater variability between wells than within a single well. The bulk mineralogy of the samples is broadly similar (Table 2).

Table 2. Whole-rock mineralogy.

Well	Depth (mbsf)	Sm	I-S	Cl	I/M	K	Qz	KFp	Plg	Ba	Cc	Ap	Do	G	Si	Other
Panis	1816		xx	x	xx	xx	xx	x	xx	o						P
Panis	1999		xx	x	o	o	xx	x	xx	x		o				P
Panis	2907		xx	o	xx		xx				x	o				Op
Panis	3090	x	xx	o	x	x	xx	o	o	o	xx					P
Ikon	4128	x	xx		xx	xx	xx		x		x	o		x		
Ikon	4418	x	xx		xx	x	xx	xx	x		xx	x		x		
Ikon	5133	x	xx		xx	xx	xx	o	x		o	o		x	x	H
Ikon	5420	x	xx		xx	x	xx	x	x		x	o		x	x	P, H
Diva	4855		xx		xx	x	xx	x	xx		x	o		x	x	P, H
Diva	5001		xx		xx	xx	xx	xx	xx		x	o		x	x	
Diva	5435		xx		x	xx	xx				xx			x	x	Op, H
Diva	5511		xx		xx	x	xx	x	xx		x	o		x	x	
Diva	5516		xx		xx	xx	xx	x	x		x	o		x	x	P, Str
Diva	5518		xx		xx	x	xx	o	xx		x	o		x	x	
Diva	5647		xx	o	xx	xx	xx	xx	xx		x	o	o	x	x	
Diva	5649		xx		xx	xx	xx	xx	xx		x	x		x	x	

xx = abundant; x = common; o = rare; Sm = smectite; I-S = mixed-layer illite-smectite; Cl = chlorite; I/M = illite/mica; K = kaolinite; Qz = quartz; KFp = K-feldspar; Plg = plagioclase; Ba = barite (drilling mud contamination); Cc = calcite; Ap = apatite; Do = dolomite; Ah = anhydrite; H = hematite; G = goethite; P = pyrite; Si = siderite; Op = opal-a/ct; Str = strontianite; mbsf = meters below sea floor

Quartz, illite/mica, kaolinite and I-S dominate; the main differences between the samples from Panis and Ikon/Diva are in the less common or ancillary minerals. In Panis samples, calcite, K-feldspar and plagioclase are common, with dolomite, apatite and pyrite as common ancillary phases. Barite occurs in several Panis samples and is believed, based on the relationship between it and organic carbon, to result from contamination from barite-containing, polymer-based drilling mud. Analyses of organic carbon suggest that the level of contamination is of the order of a few percent of the total sample. Compared to the Panis samples, calcite, siderite and goethite are more common throughout Ikon and Diva, with gypsum present in Ikon and Diva, perhaps as a result of precipitation from the highly saline porewaters related to evaporites in the section.

Clay mineralogy

The XRD patterns of the <0.2 μm and <2 μm fractions of representative samples are shown in Figure 2, with the data tabulated in Table 3. As one of the aims of this paper is to assess the effect of clay mineral recrystallization on microfabric, we are particularly interested in establishing the clay mineralogy of the samples, identifying differences in initial mineralogy as well as mineralogical change related to diagenesis.

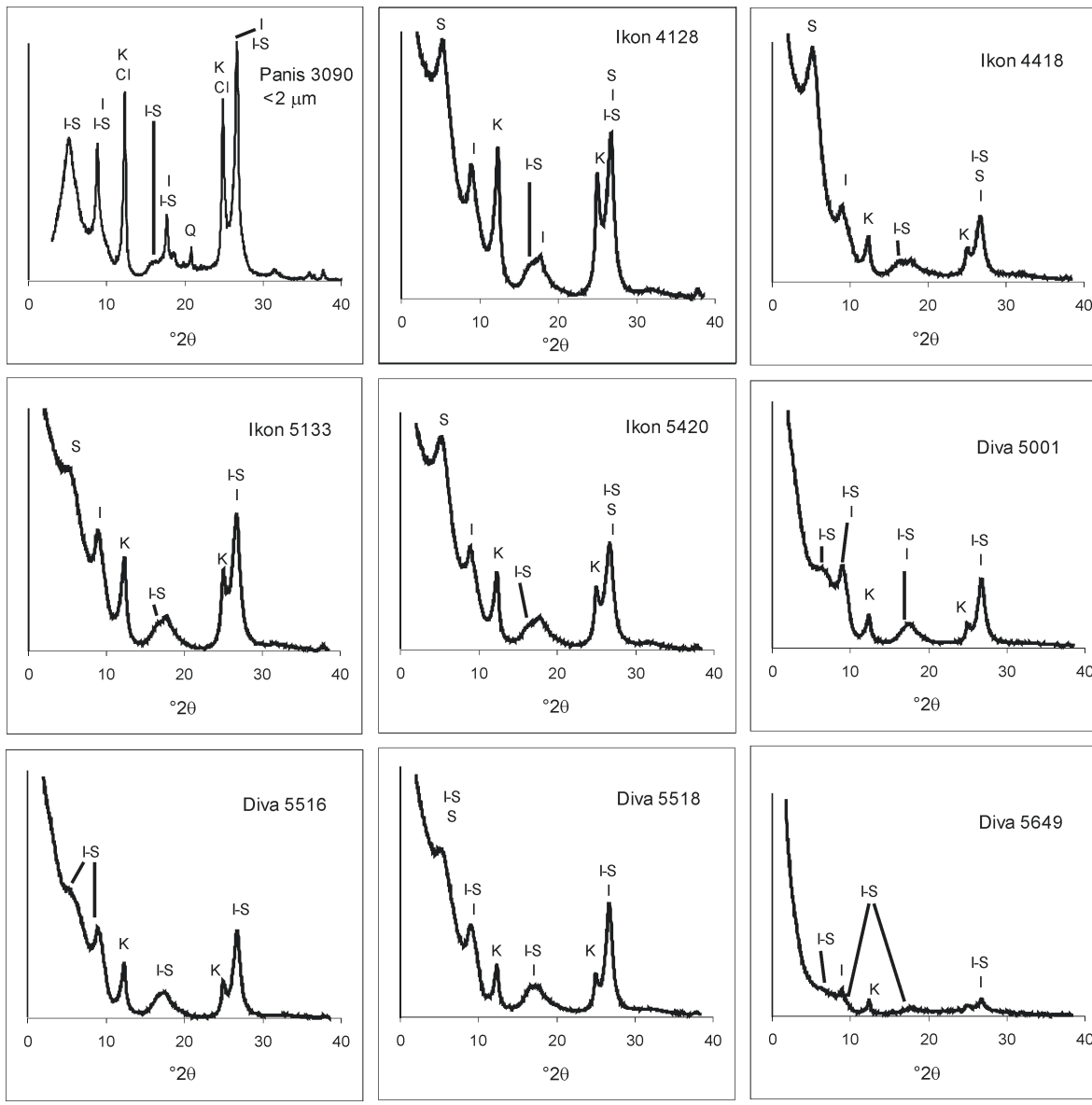

Figure 2. XRD patterns of Na-saturated, glycolated <0.2 μm (2 μm for Panis) separates of representative samples. I = illite; I-S = mixed-layer illite-smectite; K = kaolinite; Cl = chlorite; Q = quartz. See Table 3 for more details of the mineralogy.

Table 3. High-resolution X-ray texture goniometry data and clay mineralogy of the <2 μm fraction of Panis and the <0.2 μm fraction of Ikon and Diva.

Well	Depth (mbsf)	Temp (ºC)	<2 μm (%)	%S	%I	%C	%K	%R1 I-S	%S in R1 I-S	%R0 I-S	%S in R0 I-S	I-S MPD (m.r.d.)	K/C MPD (m.r.d.)
Panis	1816	40	41	0	29	8	8	36	33	0	–	–	2.73
Panis	1999	44	39	0	40	11	11	23	55	0	–	4.05	3.80
Panis	2907	64	39	0	37	5	5	36	49	0	–	2.70	2.9
Panis	3090	67	44	0	5	6	6	72	33	0	–	3.10	2.57
Ikon	4128	90	46	17	16	0	0	42	35	0	–	–	1.99
Ikon	4418	95	39	31	6	0	0	51	32	0	–	2.69	1.87
Ikon	5133	107	56	13	11	0	0	59	32	0	–	2.78	–
Ikon	5420	111	44	17	3	0	0	63	30	0	–	1.88	1.80
Ikon	5884	119	n.d.	16	6	0	0	64	38	0	–	n.d.	n.d.
Diva	4855	117	36	7	2	0	0	0	–	82	41	2.60	2.08
Diva	5001	120	49	0	2	0	0	89	25	0	–	1.74	–
Diva	5435	127	n.d.	10	4	0	0	0	–	79	35	n.d.	n.d.
Diva	5511	128	37	4	4	0	0	0	–	82	31	2.76	1.92
Diva	5516	128	33	0	0	0	0	84	33	0	–	2.17	3.36
Diva	5518	128	60	4	2	0	0	0	–	85	33	2.46	1.91
Diva	5647	130	22	0	4	0	0	86	28	0	–	n.d.	2.47
Diva	5649	130	38	0	4	0	0	85	28	0	–	3.41	2.32

MPD = maximum pole density; S = smectite; I-S = mixed-layer illite-smectite; C = chlorite; I = illite; K = kaolinite; mbsf = metres below sea-floor. n.d. = not determined

All samples contain quartz, kaolinite and illite/mica in the <2 μm fractions; Panis samples also contain chlorite. In terms of diagenetic change, we are mainly interested in mixed-layer illite-smectite (I-S). For the Panis samples, for which we only have data for <2 μm separates, a detailed interpretation of the nature of I-S minerals is compromised in some cases by the rather weak reflections and also by the substantial amount of discrete illite which hampers the precise identification of the I-S 002 and 003 reflections. However, the Panis <2 μm separates are dominated by a mixture of illite plus R1 I-S with 33–55% expandable layers, and lesser amounts of kaolinite and chlorite (Table 3). There are no trends with temperature and we view this mix as being representative of the detrital clay mineral input to the system. Note that there is no firm evidence of smectite, although it is possible that small amounts are present.

Samples from Ikon and Diva span the temperature range (90–130ºC) over which the progressive illitization of smectite is generally considered to occur (*e.g.* Hower *et al.*, 1976; Velde and Vasseur, 1992; Essene and Peacor, 1995). However, the X-ray data for the <0.2 μm separates from Ikon and Diva (Figure 2; Table 3) are not consistent with this model. Firstly, discrete smectite occurs in all samples up to 119ºC and in some samples up to 128ºC. Secondly, there is no clear-cut illitization trend with increasing temperature; samples contain either R1 or R0 I-S with 25–41% expandable layers, with the expandability almost independent of temperature (Table 3). Ikon samples (90–119ºC) all contain smectite and R1 I-S with 30–38% expandable layers. Those Diva samples (117–130ºC) which contain smectite have R0 I-S with 31–41% expandable layers; Diva samples without smectite have R1 I-S with 25–33% expandable layers.

Phyllosilicate fabric

Despite burial to 5.5 km and a reduction in porosity from a probable depositional value of ~70% to present values of 10–20%, none of the samples in this study has a strongly aligned phyllosilicate fabric, including those samples which display depositional lamination. Maximum pole densities for I-S range from 1.74 to 4.05 m.r.d. and are mainly <3 m.r.d. (Table 3). The maximum pole densities are independent of burial depth over a range of 1.5 to 5.5 km (Table 3; Figures 3, 4). The degree of preferred orientation for the kaolinite/chlorite phases is generally similar but somewhat lower than that of I-S (Table 3). The lack of an aligned phyllosilicate fabric is supported by BSEM images, which show a chaotic fabric for most of the samples (Figure 5), including the most clay-rich samples.

These results differ substantially from the findings of Ho *et al.* (1999) from the shallow-water Gulf Coast. There, a major increase in the alignment of phyllosilicates occurred across the smectite to illite transition at depths between 2 and 2.5 km (80–100ºC). In our samples from the deep-water Gulf of Mexico, smectite persists to 120ºC and there is limited support for either substantial illitization or fabric realignment. The BSEM images (Figure 5) do suggest minor rearrangement of fabric normal to the principal (vertical) stress of those deepest samples which do not contain discrete smectite. However, the maximum pole density values for the two most illitized samples are 3.15 and 3.41 m.r.d., compared to values around 6 m.r.d. in the Ho *et al.* (1999) data set.

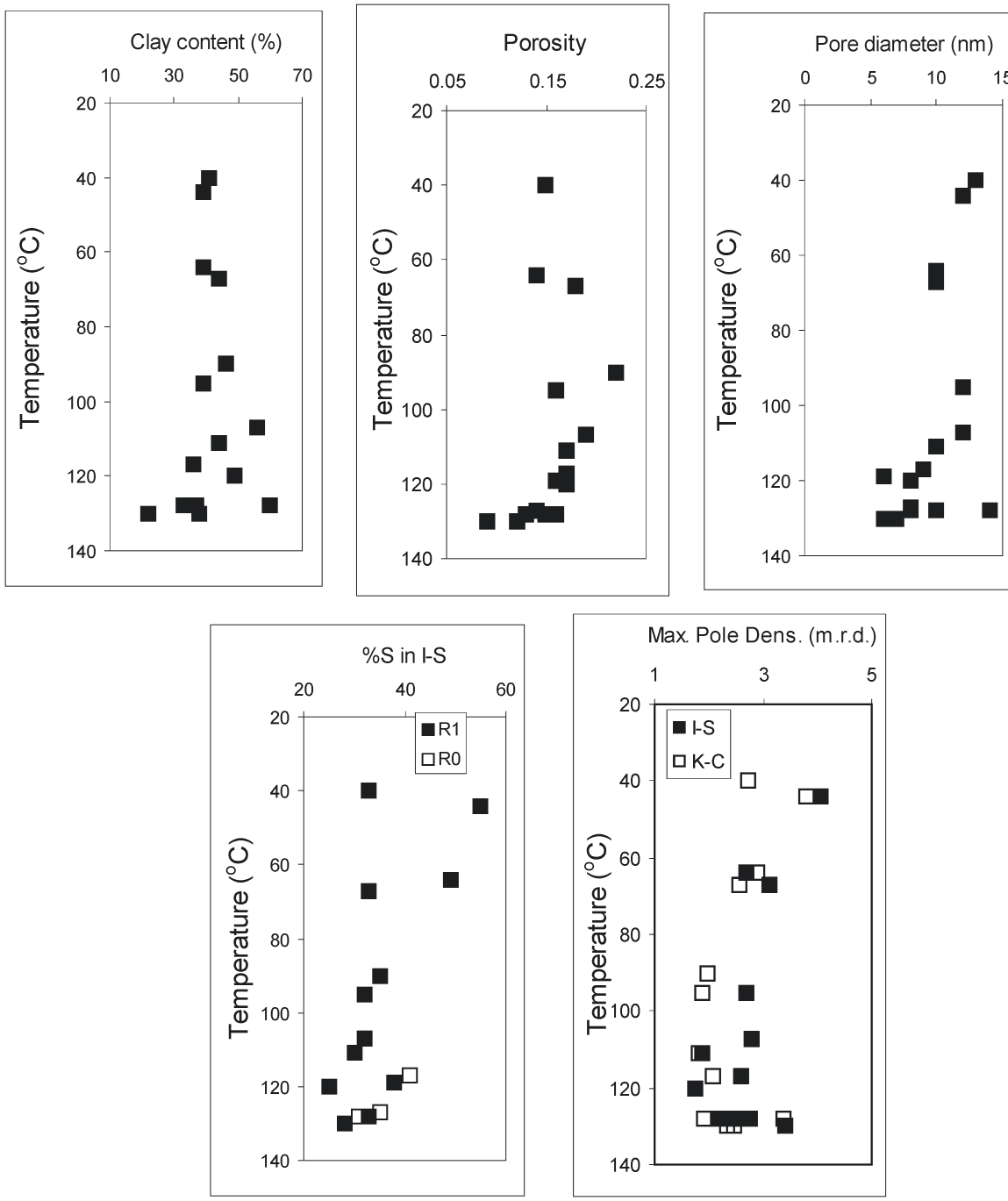

Figure 3. Physical properties of samples as a function of temperature.

Porosimetry

Porosities range from 0.09 to 0.22 and are largely independent of depth (Table 1, Figure 3). The narrow porosity range over a 4 km depth range reflects the increasing overpressure deeper into the sections. Fluid-pressure data from adjacent sandstones indicate that the vertical effective stress, the driving force for mechanical compaction, is similar throughout the section at ~20 MPa. Modal pore-throat sizes are generally between 6 and 15 nm (Table 1, Figure 3), low values which are consistent with the mudstones' compactional state and lithology (Yang and Aplin, 1998; Dewhurst *et al.*, 1999). Both porosity and pore-size distribution data thus indicate extensive compaction, with the two most

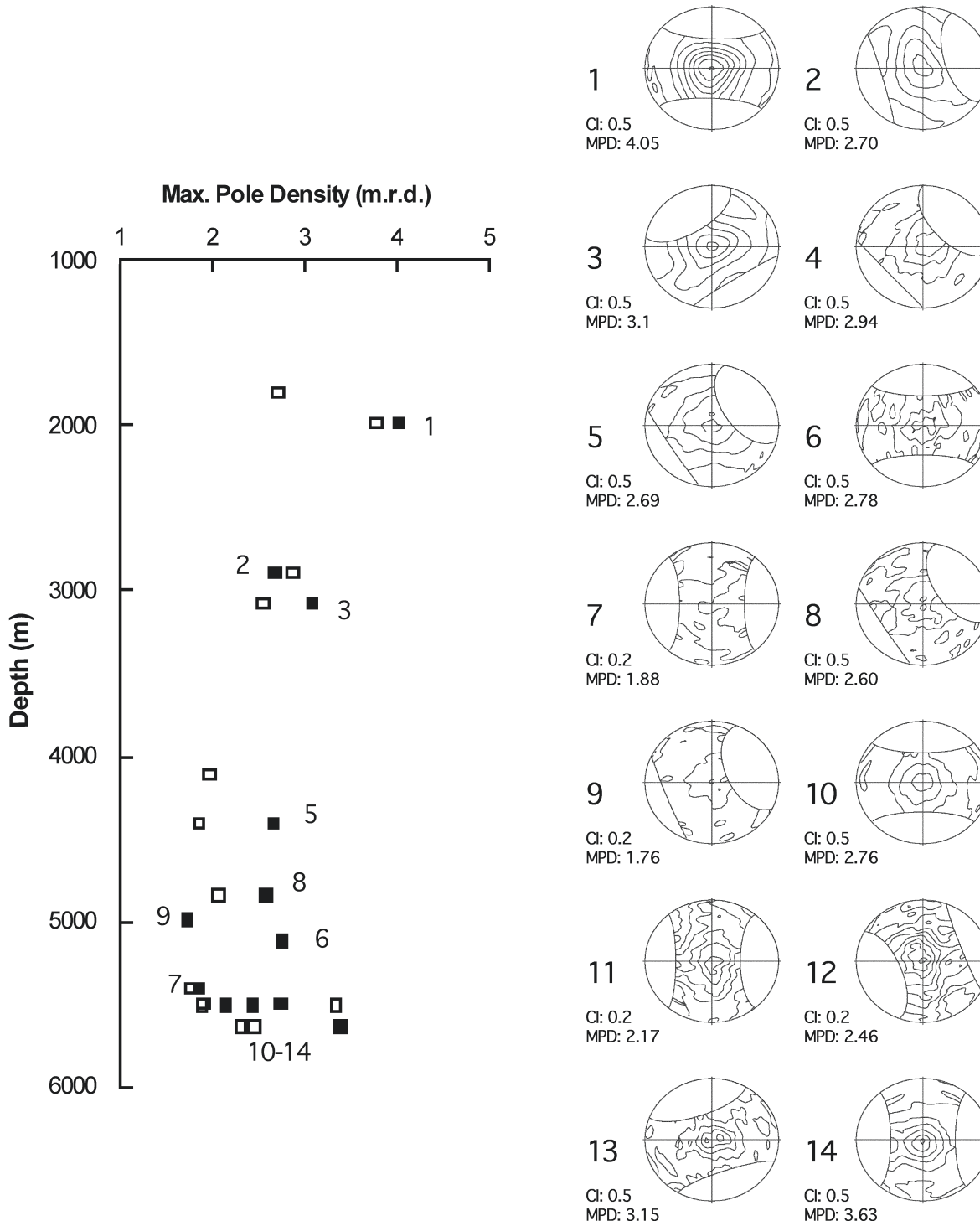

Figure 4. Maximum pole densities of phyllosilicates, expressed as multiples of a random distribution. The pole figures were rotated into the direction of the maximum intensity. CI = contour intensity; MPD = maximum pole density. Filled squares: I-S; open squares: kaolinite + chlorite. Contour interval = 0.5 for samples 1–10 and 13–14; CI = 0.2 for samples 11 and 12.

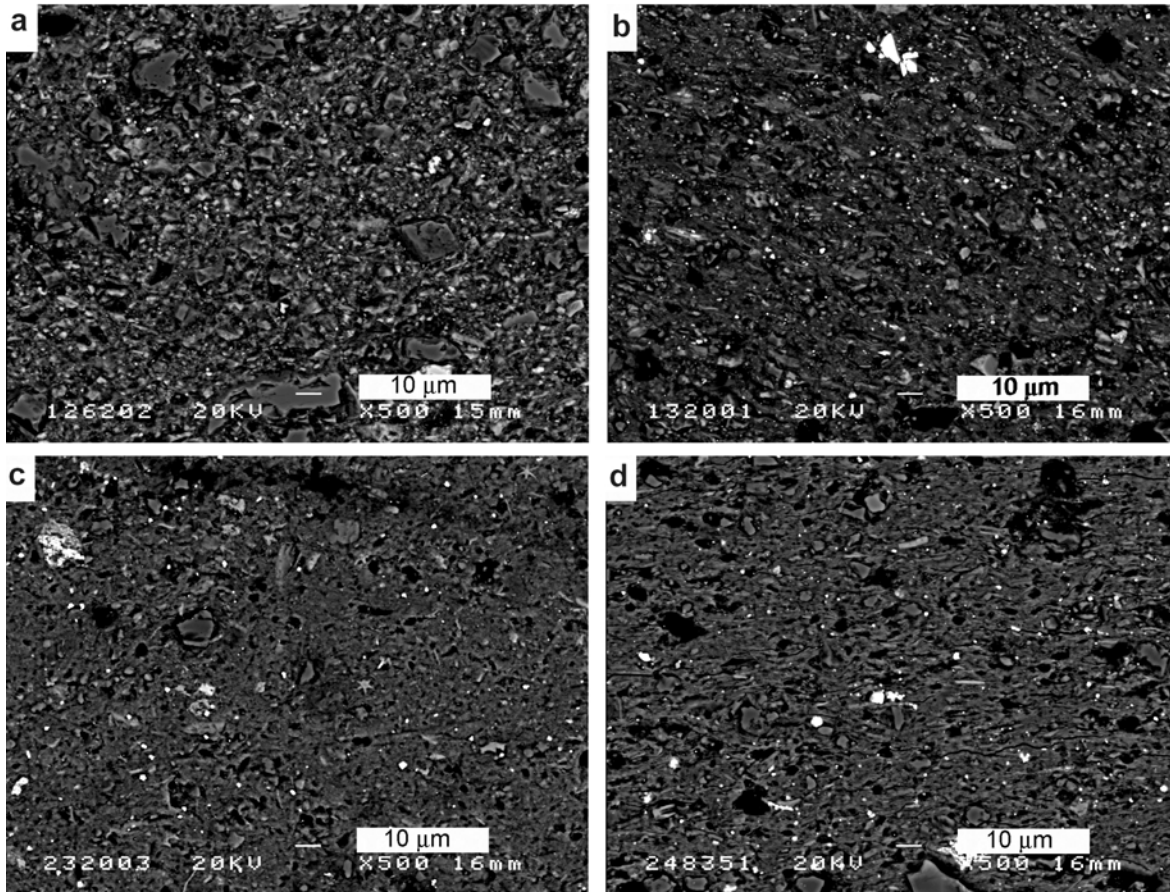

Figure 5. Backscattered electron micrographs: (a) Panis 1816 mbsf, %S in I-S ~30, maximum pole density unmeasurable due to lack of fabric; (b) Panis 1999 mbsf, %S in I-S ~55, maximum pole density = 4.05; (c) Diva 5001 mbsf, %S in I-S ~25, maximum pole density = 1.74; (d) Diva 5649 mbsf, %S in I-S ~28, maximum pole density = 3.41.

illitized samples having the lowest porosities and smallest modal pore size of all the samples.

DISCUSSION

Clay mineralogy

Many previous studies have used XRD data to describe the conversion of smectite to illite as a kinetically controlled reaction in which smectite layers are steadily converted to illite (*e.g.* Hower *et al.*, 1976; Freed and Peacor, 1989; Velde and Vasseur, 1992; Essene and Peacor, 1995; Elliott and Matisoff, 1996; Berger *et al.*, 1999). Studies in the shallow-water and onshore Gulf Coast mudstones have concluded that the formation of I-S with low expandability is generally complete at ~100ºC (*e.g.* Hower *et al.*, 1976; Kisch, 1983; Freed and Peacor, 1989). Our results are very different; in these deep-water Gulf of Mexico samples, discrete smectite persists to temperatures in excess of 120ºC and coexists with R0 and R1 I-S with only 25–40% expandable layers. We suggest that these data can be explained in one of two ways.

One possibility is that illitization of detrital I-S occurs in preference to illitization of detrital smectite. We do not favor this model because we have no evidence of detrital smectite in the more shallow-buried Panis samples (albeit of <2 µm separates) and are unable to find any support for this model in the extensive illitization literature.

The second model, which we prefer but which requires further investigation, is that the <0.2 µm I-S is detrital and that the discrete smectite is being formed by *in situ* alteration of volcanic glass. Discrete smectite coexisting with expandable I-S is not commonly recognized, but has been reported by McCarty (2005), who found that smectite was associated with I-S when volcanic glass was also present in the samples. Lanson *et al.* (2005a, 2005b) have similarly reported the coexistence of R1 I-S with relatively low expandability coexisting with R0 I-S with high expandability in the Gulf of Mexico, and Drits *et al.* (2002) suggested the coexistence of chemically and structurally distinct I-S in some mudstones from East Greenland. Drits *et al.* (2002) suggested differing origins of the two mineral types,

with the more expandable phase derived from the weathering of volcanic material. Certainly, abundant volcanic glass exists in some offshore Gulf of Mexico strata (Hunter and Davies, 1979; Hanan *et al.*, 1998), and Hanan *et al.* (1998) have traced the origin of the glass to volcanic centers in the Snake River area of the Rocky Mountains. We envisage a mechanism where smectite forms from glass and illitization is slowed until the glass is consumed, perhaps because K is unavailable for illitization through its consumption by the alteration of glass (*e.g.* Staudigel and Hart, 1983; Pichler *et al.*, 1999; Stroncik and Schminke, 2001). However, our data do not rule out limited illitization of detrital I-S. Firstly, the expandability of the I-S in the <2 μm fraction of Panis samples is somewhat greater than that of the I-S in the <0.2 μm fraction of hotter Ikon and Diva samples. Secondly, I-S in samples containing discrete smectite is more expandable (30−41% S) than in samples without discrete smectite (25−33% S). Our argument is thus that the formation of smectite from glass slows down rather than halts the illitization reactions. More details of this interpretation will be presented in future work.

Although we do not have sufficient data to undertake a rigorous analysis of the kinetics of putative reactions involving smectite in this section, it is noteworthy that compared to onshore Gulf Coast sections, the mudstones in this study are young (Pliocene-Miocene) and have been subjected both to rapid burial (up to 1000 m/my) and a low thermal gradient (20−23ºC/km). In addition to the occurrence of volcanic glass, the apparently high temperature of illitization could also reflect the time-temperature history of the sediments. The high temperature at which illitization occurs in this section is similar to that observed in the South Caspian Basin (Buryakovsky *et al.*, 1995), where similar age sediments (Miocene–Pliocene) have had a similar thermal history (current thermal gradients 15−20ºC/km).

Phyllosilicate fabric

The fabric data (Table 3, Figures 4, 6) show that maximum pole densities range from very weak (<2 m.r.d.) to moderate (3−4 m.r.d.) and, even in the hottest and deepest samples, never reach the values of 5−6 m.r.d. measured by Ho *et al.* (1999) in lower-temperature samples from the coastal Gulf of Mexico section. These results are qualitatively consistent with the BSEM images which show little evidence of aligned fabrics, except for the two samples at 130ºC, where some fabric is implied by the parallel orientations of cracks resulting from the unloading that occurs when cores are brought to surface conditions.

Since there is substantial evidence that both mechanical compaction (*e.g.* Bowles *et al.*, 1969; Bennett *et al.*, 1981; Vasseur *et al.*, 1995) and clay mineral recrystallization (*e.g.* Ho *et al.*, 1999) can result in the development of a strongly aligned phyllosilicate fabric, we need to explore why this is not the case in these sediments. It is indeed counter-intuitive that intense mechanical compaction does not result in substantial reorientation of platy minerals. One issue relates to the scale of observation. Whereas HRXTG quantitatively determines the alignment of phyllosilicates of an oriented section over an area of 1 mm^2, most previous studies have qualitatively examined mudstone microfabric using electron micrographs imaging an area of ~0.01 mm^2, within a sample that is not oriented relative to the stress field. It is possible that a strongly aligned fabric might exist on a 0.01 mm^2 scale but not a 1 mm^2 scale. For example, Curtis *et al.* (1980) stressed the importance of quartz silt in inhibiting the development of a strongly aligned phyllosilicate fabric in mudstones. In that situation, clusters of phyllosilicates could produce a locally aligned fabric observable by SEM but which would be randomized around equidimensional quartz grains on the millimetre scale. The importance of the ratio of phyllosilicates to more equidimensional grains on fabric alignment is clearly observed in the Ho *et al.* (1999) dataset, in which millimetre-scale phyllosilicate fabric intensities are much lower in samples rich in detrital quartz grains (Figure 6).

In this sample set, however, grain size and mineralogical analysis show that fabric is weak or moderate even in the most clay-rich samples, and even in illitized samples. We propose that the lack of an aligned fabric in these samples reflects a combination of (1) the way in which the phyllosilicate particles were deposited and (2) the limited extent of phyllosilicate diagenesis, especially illitization of smectite. As it is inconceivable that a phyllosilicate fabric would decrease as a function of increasing burial and effective stress, we infer from the lack of an aligned phyllosilicate fabric at 3−4 km burial depth that the phyllosilicates in these mudstones were deposited without a preferred orientation, whatever

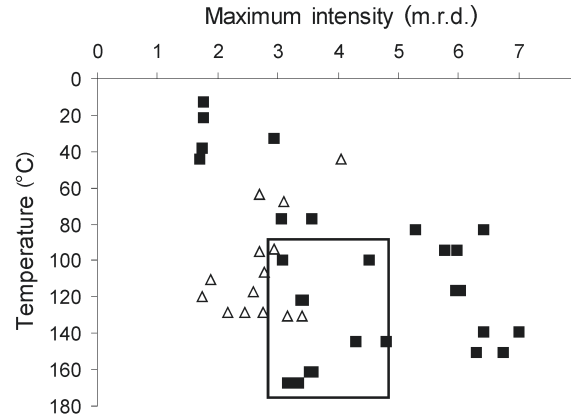

Figure 6. Comparison of the maximum pole densities of the samples from this study and those from the onshore Gulf of Mexico (Ho *et al.*, 1999). 'Sandy' samples from the study by Ho *et al.* study are within the box and are described as containing significant amounts of silt and sand-grade quartz. In the study by Ho *et al.*, the S to I transition occurs between ~80 and 100ºC.

the precise nature of the processes of sediment deposition. It is also important to note that phyllosilicates do not show a preferred alignment even in samples with clear depositional lamination. The data presented here are consistent with work in the modern Mississippi Delta which suggests that the primary depositional texture of phyllosilicates in surficial muds is generally random with common edge-to-face grain contacts, suggesting the importance of flocculation in the deposition of phyllosilicates (Bennett *et al.*, 1991).

Without a preferentially aligned, depositional phyllosilicate fabric, mechanical compaction of these mudstones to porosities of ~15% and an effective stress of 20 MPa (2900 psia) has not resulted in a substantial reorientation of phyllosilicates normal to the maximum stress. Whilst this may in part reflect variations in the local stress field imposed by quartz grains, electron micrographs do not reveal an oriented fabric even in clay-rich areas where equidimensional quartz grains are rare. We conclude that isotropic phyllosilicate fabrics can be preserved even after very substantial mechanical compaction.

Ho *et al.* (1999) presented evidence for a major reorganization of phyllosilicate fabric related to the smectite to illite transition in shallow water Gulf Coast mudstones. Their data are plotted along with our results in Figure 6. In what Ho *et al.* (1999) described as fine-grained samples, maximum pole densities increase abruptly from ~3 to between 6 and 7 across the transition. In our samples, maximum pole densities do not exceed 3.5, even at the base of the section where there is no discrete smectite and where the %I in I-S is ~70–75%. Although Ho *et al.* (1999) observed that fabric intensities at a given temperature were much lower in 'sandy' samples than in fine-grained samples (*cf.* Curtis *et al.*, 1980), the relatively weak fabric in our samples cannot be ascribed to the occurrence of silt-grade quartz, as most of our samples are fine-grained, with clay fractions in excess of 40%. We suggest that the lack of a strongly aligned phyllosilicate fabric reflects the apparently limited extent of illitization that these mudstones have been subjected to. We propose a two-stage diagenetic process involving (1) the alteration of volcanic glass/ash to smectite, and (2) the illitization of smectite and I-S. The alteration of glass results in smectite without a preferred orientation and retards the illitization reaction. Based on the shallower Panis samples, we propose that the detrital I-S supplied to these sediments was quite illitic and that the low expandability of I-S in the hottest section is the result of only modest illitization and recrystallization. Based on a host of studies of shales and metamorphic pelites, we suggest that the recrystallization and growth of illite will continue with increasing thermal stress, documenting the process by which muds are converted into shales and pelites, with an attendant enhancement of fabric (*e.g.* Lee *et al.*, 1985; Peacor, 1992; Merriman and Peacor, 1999). The samples in this study are documenting (1) mechanical compaction processes and (2) a relatively early phase of recrystallization, neither of which have led to a substantial realignment of phyllosilicates, at least on the square millimetre scale observed by HRXTG.

Non-mechanical compaction

Non-mechanical compaction (pressure solution, stylolitization) is the process by which porosity is reduced through mineral dissolution at grain contacts, independent of effective stress. It is a well known phenomenon in both carbonates and sandstones (*e.g.* Garrison and Kennedy, 1977; Tada and Siever, 1989; Bjørkum, 1996) but is much less well documented in muds, partly because the small grain size of mudstones makes petrography difficult, and partly because of the difficulty of establishing an accurate baseline for purely mechanical compaction. Because the porosity-effective stress relationships of muds vary according to lithology or grain size (Burland 1990; Aplin *et al.*, 1995; Yang and Aplin, 2004), one must be certain that any change in porosity observed across a zone of mineralogical or chemical change can be related to the mineralogical event and not inherited from lithological difference.

Figure 3 displays porosity, pore radius, fabric and mineralogy as a function of both depth and *in situ* formation temperature. There are no significant changes in porosity or modal pore-throat size between 2000 mbsf (40ºC) and 5000 mbsf (120ºC), with porosities close to the 15% value suggested by several authors to be the minimum value achievable by mechanical compaction alone (Brown and Ransom, 1996; Lahann, 2002). At depths >5000 mbsf (120ºC), coincident with the disappearance of discrete smectite and the increase in %I in I-S from 60–70 to 70–75%, porosity drops from ~15% to <10% at 5649 mbsf (130ºC). Trends in the modal pore size are less clear but the two most illitized samples have the smallest modal pore-throat size (~6 nm). Because the S to I transition occurs over a relatively narrow range of effective stress, the dataset should be ideal for unraveling the relative effects of illitization and lithology on compaction. However, although it is tempting to suggest that the abrupt reduction in porosity has been caused by illitization at a constant effective stress, as previously suggested by Lahann *et al.* (2001) and Lahann (2002), the dataset is too small to allow strong conclusions to be drawn. The five samples above 120ºC have clay fractions ranging between 22 and 60%, which would result in different porosities simply as a result of mechanical compaction (Yang and Aplin, 2004). Coarser-grained samples would be expected to have lower porosities, which is broadly what we observe. Whether or not there is an additional non-mechanical effect contributing to porosity and permeability, reduction must be decided on an expanded dataset.

CONCLUSIONS

At deposition, the phyllosilicate fabric of the mudstones described in this study was weak or isotropic. Intense mechanical compaction has reduced their porosity from ~75 to 15% but has not resulted in a strongly aligned phyllosilicate fabric, even in fine-grained, clay-rich samples.

Unusually, discrete smectite persists in <0.2 μm separates to ~120ºC, coexisting with R1 I-S or R0 I-S with 30–40% expandable layers. Between 120 and 130ºC, discrete smectite disappears and the expandability of I-S decreases to ~25–30%. We propose a two-stage diagenetic process involving (1) the alteration of volcanic glass/ash to smectite, and (2) the illitization of smectite and I-S. The alteration of glass results in smectite without a preferred orientation and retards the illitization reaction. The lack of a strongly aligned phyllosilicate fabric is thus thought to reflect the apparently limited extent of illitization, and thus recrystallization, to which these mudstones have been subjected.

We anticipated that this dataset would help us determine whether mudstone porosity and permeability was reduced by non-mechanical processes, primarily the conversion of smectite to illite. In these samples, mechanical compaction is indeed the dominant mechanism by which porosity is lost. However, there is a hint that clay mineral recrystallization might further reduce porosity. A larger dataset is required to enhance confidence in this hypothesis.

ACKNOWLEDGMENTS

This work was generously supported by the GeoPOP industrial consortium comprising Amerada Hess, BG, BP, ChevronTexaco, ConocoPhillips, ExxonMobil, JNOC, Norsk Hydro, Shell, Statoil and Total, and precursors of those companies. We particularly thank Richard Lahann and an anonymous reviewer for their very important comments on the manuscript. Steve Hillier generously performed part of the clay mineralogy and Joe Macquaker kindly helped with the SEM.

REFERENCES

Aplin, A.C., Yang, Y.L. and Hansen, S. (1995) Assessment of beta, the compression coefficient of mudstones and its relationship with detailed lithology. *Marine and Petroleum Geology*, **12**, 955–963.

Bennett, R.H., Bryant, W.R. and Keller, G.H. (1981) Clay fabric of selected submarine sediments: fundamental properties and models. *Journal of Sedimentary Petrology*, **51**, 217–232.

Bennett, R.H., O'Brien, N.R. and Hulbert, M.H. (1991) Determinants of clay and shale microfabric signatures: processes and mechanisms. Pp. 5–32 in: *Microstructure of Fine-Grained Sediments* (R.H. Bennett, N.R. O'Brien and M.H. Hulbert, editors). Springer-Verlag, New York.

Berger, G., Velde, B. and Aigouy, T. (1999) Potassium sources and illitization in Texas Gulf Coast shale diagenesis. *Journal of Sedimentary Research*, **69**, 151–157.

Bjørkum, P.A. (1996) How important is pressure in causing dissolution of quartz in sandstones? *Journal of Sedimentary Research*, **66**, 147–154.

Bowles, F.A., Bryant, W.R. and Wallin, C. (1969) Microstructure of unconsolidated and consolidated marine sediments. *Journal of Sedimentary Petrology*, **39**, 1546–1551.

British Standards 733, part 2 (1987) *Pyknometers. Part 2. Methods for calibration and use of pyknometers*. British Standards Institution, London.

British Standards 1377, part 6 (1990) *Method of Test for Soils for Civil Engineering Purpose*. British Standards Institution, London.

Brown, K.M. and Ransom, B. (1996) Porosity corrections for smectite-rich sediments: Impact on studies of compaction, fluid generation, and tectonic history. *Geology*, **24**, 843–846.

Burland, J.B. (1990) On the compressibility and shear strength of natural clays. *Géotechnique*, **40**, 329–378.

Buryakovsky, L.A., Djevanshir, R.D. and Chilingar, G.V. (1995) Abnormally-high formation pressures in Azerbaijan and the South Caspian Basin (as related to smectite ↔ illite transformation during diagenesis and catagenesis). *Journal of Petroleum Science and Engineering*, **13**, 203–218.

Curtis, C.D., Lipshie, S.R., Oertel, G. and Pearson, M.J. (1980) Clay orientation in some Upper Carboniferous mudrocks, its relationship to quartz content and some inferences about fissility, porosity and compactional history. *Sedimentology*, **27**, 333–339.

Delage, P. and Lefebvre, G. (1984) Study of a sensitive Champlain Clay and its evolution during consolidation. *Canadian Geotechnical Journal*, **21**, 21–35.

Dewhurst, D.N., Aplin, A.C. and Sarda, J.P. (1999) Influence of clay fraction on pore-scale properties and hydraulic conductivity of experimentally compacted mudstones. *Journal of Geophysical Research*, **104**, 29261–29274.

Drits, V.A. and Sakharov, B.A. (1976) *X-ray Structure Analysis of Interstratified Minerals*, Nauka, Moscow, 256 pp. (in Russian).

Drits, V.A. and Tchoubar, C. (1990) *X-ray Diffraction by Disordered Lamellar Structures.* Springer-Verlag, Berlin, 371 pp.

Drits, V.A., Lindgreen, H. and Salyn, A. (1997a) Determination by X-ray diffraction of content and distribution of fixed ammonium in illite-smectite. Application to North Sea illite-smectites. *American Mineralogist*, **82**, 79–87.

Drits, V.A., Sakharov, B.A., Lindgreen, H. and Salyn, A. (1997b) Sequential structure transformation of illite-smectite-vermiculite during diagenesis of Upper Jurassic shales from the North Sea and Denmark. *Clay Minerals*, **32**, 351–371.

Drits, V.A., Sakharov, B.A., Dainyak, L.G., Salyn, A.L. and Lindgreen, H. (2002) Structural and chemical heterogeneity of illite-smectite from Upper Jurassic mudstones of East Greenland related to volcanic and weathered parent rocks. *American Mineralogist*, **87**, 1590–1607.

Elliott, W.C. and Matisoff, G. (1996) Evaluation of kinetic models for the smectite to illite transformation. *Clays and Clay Minerals*, **44**, 77–87.

Essene, E.J. and Peacor, D.R. (1995) Clay mineral thermometry – a critical perspective. *Clays and Clay Minerals*, **43**, 540–553.

Freed, R.L. and Peacor, D.R. (1989) Variability in temperature of the smectite/illite reaction in Gulf Coast sediments. *Clay Minerals*, **24**, 171–180.

Garrison, R.E. and Kennedy, W.J. (1977) Origin of solution seams and flaser structures in the Upper Cretaceous chalks of southern England. *Sedimentary Geology*, **19**, 107–137.

Hampton, M.A., Lee, H.J. and Locat, J. (1996) Submarine landslides. *Reviews of Geophysics*, **34**, 33–59.

Hanan, M.A., Totten, M.W., Hanan, B.B. and Kratochovil, T. (1998) Improved regional ties to global geochronology using Pb-isotope signatures of volcanic glass shards from deep water Gulf of Mexico ash beds. *Transactions - Gulf Coast Association of Geological Societies*, **48**, 95–105.

Hedberg, H.D. (1936) Gravitational compaction of clays and shales. *American Journal of Science*, **31**, 241–287.

Ho, N.C., Peacor, D.R. and van der Pluijm, B.A. (1995) Reorientation of phyllosilicates in the mudstone-to-slate transition at Lehigh Gap, Pennsylvania. *Journal of Structural Geology*, **17**, 345–356.

Ho, N.C., Peacor, D.R. and van der Pluijm, B.A. (1996) Contrasting roles of detrital and authigenic phyllosilicates during slaty cleavage development. *Journal of Structural Geology*, **18**, 615–623.

Ho, N.C., Peacor, D.R. and van der Pluijm, B.A. (1999) Preferred orientation of phyllosilicates in Gulf Coast mudstones and relation to the smectite-to-illite transition. *Clays and Clay Minerals*, **47**, 495–504.

Ho, N.C., van der Pluijm, B.A. and Peacor, D.R. (2001) Static recrystallisation and preferred orientation of phyllosilicates: Michigamme Formation, northern Michigan. *Journal of Structural Geology*, **23**, 887–893.

Hower, J., Eslinger, E.V., Hower, M.E. and Perry, E.A. (1976) Mechanism of burial metamorphism of argillaceous sediment: 1. Mineralogical and chemical evidence. *Geological Society of America Bulletin*, **87**, 725–737.

Hunter, B.E. and Davies, D.K (1979) Distribution of volcanic sediments in the Gulf Coastal Province – significance to petroleum geology. *Transactions - Gulf Coast Association of Geological Societies*, **29**, 147–155.

Jacob, G., Kisch, H.J. and van der Pluijm, B.A. (2000) The relationship of phyllosilicate orientation, X-ray diffraction intensity ratios, and c/b fissility ratios in metasedimentary rocks of the Helvetic zone of the Swiss Alps and the Caledonides of Jaemtland, central western Sweden. *Journal of Structural Geology*, **22**, 245–258.

Kisch, H.J. (1983) Mineralogy and petrology of burial diagenesis (burial metamorphism) and incipient metamorphism in clastic rocks. Pp. 289–493 in: *Diagenesis in Sediments and Sedimentary Rocks II* (G. Larsen and G.V. Chilingar, editors). Developments in Sedimentology **25B**, Elsevier, Amsterdam.

Kranck, K., Smith, P.C. and Milligan, T.G. (1996a) Grain-size characteristics of fine-grained unflocculated sediments. 1. 'One-round' distributions. *Sedimentology*, **43**, 589–596.

Kranck, K., Smith, P.C. and Milligan, T.G. (1996b) Grain-size characteristics of fine-grained unflocculated sediments. 2. 'Multi-round' distributions. *Sedimentology*, **43**, 597–606.

Lahann, R. (2002) Impact of smectite diagenesis on compaction modeling and compaction equilibrium. Pp. 61–72 in: *American Association of Petroleum Geologists Memoir 76: Pressure Regimes in Sedimentary Basins and their Prediction* (A.R. Huffman and G.L. Bowers, editors). American Association of Petroleum Geologists, Tulsa, Oklahoma.

Lahann, R., McCarty, D.K. and Hsieh, J.C.C. (2001) Influence of clay diagenesis on shale velocities and fluid-pressure. *Offshore Technology Conference Paper 13046*.

Lanson, B., Sakharov, B.A., Claret, F. and Drits, V.A. (2005a) Diagenetic evolution of clay minerals in Gulf Coast shales: New insights from X-ray diffraction profile modeling. *42nd annual meeting of the Clay Minerals Society, Burlington, Vermont, Program & Abstracts*, p. 69.

Lanson, B., Sakharov, B.A., Claret, F. and Drits, V.A. (2005b) Diagenetic evolution of clay minerals in Gulf Coast shales: New insights from X-ray diffraction profile modeling. *13th International Clay Conference, Tokyo, Japan, Program & Abstracts*, pp. 39–40.

Lee, J.H., Ahn, J.H. and Peacor, D.R. (1985) Textures in layered silicates: progressive changes through diagenesis and low-temperature metamorphism. *Journal of Sedimentary Petrology*, **55**, 532–540.

Lindsay, J.F., Prior, D.B. and Coleman, J.M. (1984) Distributary-Mouth Bar development and role of submarine landslides in delta-growth, South Pass, Mississippi-Delta. *American Association of Petroleum Geologists Bulletin*, **68**, 1732–1743.

McCarty, D.K. (2005) XRD pattern simulation of clays and geological interpretation. *Clay Minerals Society Annual meeting, Burlington, Vermont. Abstract with program*.

McCarty, D.K., Drits, V.A., Sakharov, B., Zvyagina, B.B., Ruffell, A. and Wach, G. (2004) Heterogeneous mixed-layer clays from the Cretaceous Greensand, Isle of Wight, southern England. *Clays and Clay Minerals*, **52**, 552–575.

Merriman, R.J. and Peacor, D.R. (1999) Very low-grade metapelites: mineralogy, microfabrics and measuring reaction progress. Pp. 10–60 in *Low-Grade Metamorphism* (M. Frey and D. Robinson, editors). Blackwell Science, Oxford, UK.

Moore, D.M. and Reynolds, R.C. Jr. (1997) *X-ray Diffraction and the Identification and Analysis of Clay Minerals*. Oxford University Press, Oxford, UK.

Oertel, G. (1983) The relationship of strain and preferred orientation of phyllosilicate grains in rocks – a review. *Tectonophysics*, **100**, 413–447.

Oertel, G. and Curtis, C.D. (1972) Clay-ironstone concretion preserving fabrics due to progressive compaction. *Geological Society of America Bulletin*, **83**, 2597–2606.

Peacor, D.R. (1992) Diagenesis and low-grade metamorphism of shales and slates. Pp. 335–380 in: *Minerals and Reactions at the Atomic Scale* (P.R. Buseck, editor). Review in Mineralogy, **27**, Mineralogical Society of America, Washington, D.C.

Pichler, T., Ridley, W.I. and Nelson, E. (1999) Low-temperature alteration of dredged volcanics from the Southern Chile Ridge: additional information about early stages of seafloor weathering. *Marine Geology*, **159**, 155–177.

Sakharov, B.A., Lindgreen, H., Salyn, A.L. and Drits, V.A. (1999) Determination of illite-smectite structures using multispecimen XRD profile fitting. *Clays and Clay Minerals*, **47**, 555–566.

Schwab, W.C., Lee, H.J., Twitchell, D.C., Locat, J., Nelson, C.H., McArthur, W.G. and Kenyon, N.H. (1996) Sediment mass-flow processes on a depositional lobe, outer Mississippi fan. *Journal of Sedimentary Research*, **66**, 916–927.

Staudigel, H. and Hart, S.R. (1983) Alteration of basaltic glass – mechanisms and significance for the oceanic-crust seawater budget. *Geochimica et Cosmochimica Acta*, **47**, 337–350.

Stroncik, N.A. and Schmincke, H.U. (2001) Evolution of palagonite: Crystallization, chemical changes, and element budget. *Geochemistry Geophysics Geosystems 2*: Art. No. 2000GC000102.

Tada, R. and Siever, R. (1989) Pressure solution during diagenesis. *Annual Reviews in Earth and Planetary Science*, **17**, 89–118.

van der Pluijm, B.A., Ho, N. and Peacor, D.R. (1994) High-resolution X-ray texture goniometry. *Journal of Structural Geology*, **16**, 1029–1032.

Vasseur, G., Djeran-Maigre, I., Grunberger, D., Rousset, G., Tessier, D. and Velde, B. (1995) Evolution of structural and physical parameters of clays during experimental compaction. *Marine and Petroleum Geology*, **12**, 941–954.

Velde, B. and Vasseur, G. (1992) Estimation of the diagenetic smectite to illite transformation in time-temperature space. *American Mineralogist*, **77**, 967–976.

Yang, Y.L. and Aplin, A.C. (1997) A method for the disaggregation of mudstones. *Sedimentology*, **44**, 559–562.

Yang, Y.L. and Aplin, A.C. (1998) Influence of lithology and compaction on the pore size distribution and modeled permeability of some mudstones from the Norwegian margin. *Marine and Petroleum Geology*, **15**, 163–175.

Yang, Y.L. and Aplin, A.C. (2004) Definition and practical application of mudstone porosity – effective stress relationships. *Petroleum Geoscience*, **10**, 153–162.

(*Received 13 October 2003; revised 13 January 2006; Ms. 844*)